Acta Acustica 2022, **6**, 11

https://doi.org/10.1051/aacus/2022007

Available online at:
https://acta-acustica.edpsciences.org

SHORT COMMUNICATION OPEN ACCESS

Anti-reflection cover to control acoustic intensity in *in vitro* low-intensity ultrasound stimulation of cells

Meysam Majnooni[1,2], Elise Doveri[3], Jeanne Baldisser[3], Vincent Long[3], Julien Houles[4], Jean-Claude Scimeca[5], David Momier[5], Carine Guivier-Curien[1], Philippe Lasaygues[3,*], and Cécile Baron[1,2]

[1] Aix Marseille Univ, CNRS, Centrale Marseille, IRPHE UMR 7342, 13013 Marseille, France
[2] Aix Marseille Univ, CNRS, ISM UMR 7287, 13009 Marseille, France
[3] Aix Marseille Univ, CNRS, Centrale Marseille, LMA UMR 7031, 13013 Marseille, France
[4] Aix Marseille Univ, CNRS/IN2P3, CPPM UMR 7346, 13009 Marseille, France
[5] Université Côte d'Azur, CNRS, Inserm, iBV, 06108 Nice, France

Received 12 November 2021, Accepted 21 February 2022

Abstract – Low-intensity ultrasound stimulation is a technique used in therapeutic ultrasound for bone regeneration. However, the underlying mechanisms are still poorly understood. *In vitro* studies on cell cultures are implemented to understand the processes involved. To analyze the effects of ultrasonic waves on cells, the control of the delivered acoustic intensity is essential. However, depending on the insonification protocol chosen, multiple reflections and standing waves that form inside the culture medium strongly hinder the estimates. In this work, we propose the development and the experimental validation of an anti-reflection cover. We demonstrate that this custom-designed device is effective in avoiding multiple reflections and makes it possible to artificially replace the layer of culture medium with a large amount of water. Finally, an analytical study of the acoustic intensity delivered to the cells is proposed.

Keywords: Ultrasound stimulation, Cell-free culture medium, Acoustic intensity, Anti-reflection cover

1 Introduction

Therapeutic ultrasound [1–3] refers to the use of mechanical acoustic waves for treating a variety of biological tissue pathologies. More precisely, these acoustic waves can be classified into three categories depending on their intensities: waves of extreme intensities, namely shock waves (>10 kW/cm^2) used, for example, in lithotripsy or histotripsy; high-intensity waves (1–10 kW/cm^2) used, for example, for the destruction of tumors by High-Intensity Focused Ultrasound (HIFU); and low-intensity waves (<1 kW/cm^2) capable of stimulating cell growth and assisting, for example, in the healing of fractures. This work focuses on this latter application of therapeutic ultrasound.

Low-intensity ultrasound stimulation (LIUS) of bone regeneration has been demonstrated since the 1950s. There are several small and portable devices, such as the commercial Exogen™ device (Bioventus Inc, Durham, NC, USA), that patients can apply directly to the skin over the site of a bone fracture. Both fundamental research and clinical studies have been conducted to investigate the mechanical and biological effects of ultrasonic waves on cells and tissue [4], yet some of the underlying physical mechanisms involved are still poorly understood. The effectiveness of the treatment using LIUS is still discussed today [5–7]. Laboratory tests with controlled [8] and/or specific experimental setups [9, 10] are performed on cells grown in a Petri dish placed above or below a transducer. Although the transducer-cell distance and position can be adapted from one configuration to another, depending on the range of ultrasonic frequencies and the shape and orientation of the beam, reflections generally occur between the bottom of the Petri dish and the upper interface formed by the air, creating standing waves in the cell culture medium. The formation of standing waves inside the Petri dish of the *in vitro* LIUS device is a challenging problem that prevents accurate prediction of exposure conditions of the cells. This limitation of numerous *in-vitro* ultrasound stimulation protocols is often mentioned in the literature [11–13] and some technical solutions are proposed [14–17] but without examining their effectiveness, except a very recent paper [10].

2 Context & objectives

Our work focused on the development and the experimental validation of an anti-reflection cover placed over a Petri dish, under LIUS conditions in terms of frequencies,

*Corresponding author: lasaygues@lma.cnrs-mrs.fr

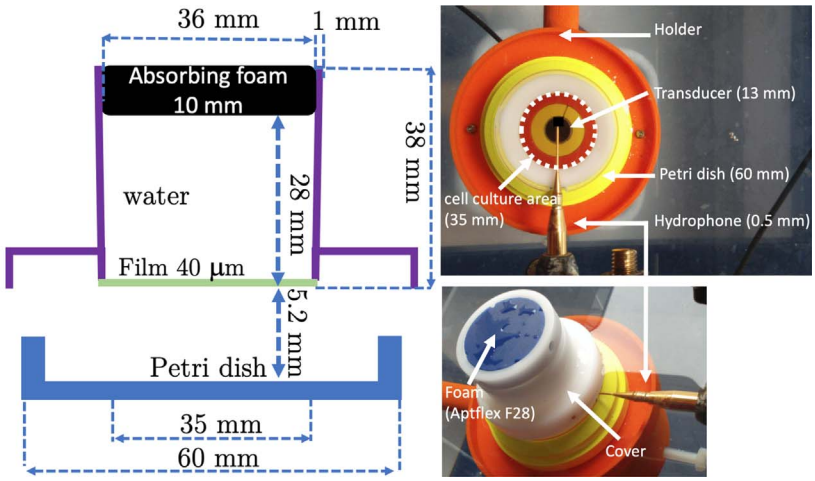

Figure 1. Schematic drawing and pictures of the Petri dish/anti-reflection cover set.

acoustic signal signatures, pressures and intensities. The Petri dish contained a cell-free degassed water layer as a hypothetical culture medium.

The tests were conducted using immersion transducers with center frequencies of 1 MHz and 2.25 MHz that were calibrated prior to the anti-reflection cover tests. These calibrations were performed in short-pulse mode, and the cover tests were performed in tone-burst mode under LIUS conditions. For both transducers, we studied the acoustic intensities with and without the Petri dish to verify intensity distributions and levels. Reflection and transmission coefficients, peak acoustic pressures, and acoustic intensities were measured and calculated for the different configurations. The custom-designed anti-reflection cover proposed in this work reduced the reflection of the waves at the interface between water and air, trapped the transmitted waves, and thus prevented the standing waves in the Petri dish water layer. We investigated how the cover over the Petri dish can influence the peak acoustic pressure. We showed that the acoustic intensity distribution and level obtained with the cover on the Petri dish containing a millimetric water layer are equivalent to those which would be measured if the Petri dish contained a high water column of several centimeters in height. We demonstrated that it is possible to analytically estimate the energy transmitted into the Petri dish and received by the cells exposed to a low intensity ultrasound field.

3 The Petri dish/anti-reflection cover set

Figure 1 shows the details, dimensions and pictures of the Petri dish/anti-reflection cover set.

The Petri dish used in the set was a Corning model (ref. 430 196) with a diameter of 60 mm, a depth of 15 mm and a wall thickness of 0.8 mm. The material the Petri dish is made of was polystyrene, with a mass density (ρ_{dish}) of 1040 kg/m^3. The ultrasonic wave velocity (c_{dish}) was measured at 2367 m/s using the method described in [18]. The attenuation (α_{dish}) of the ultrasonic waves in the material was about 1.1 dB/cm at 1 MHz, and 1.25 dB/cm at 2.25 MHz.

The anti-reflection cover was a custom-designed 38 mm-high thermoplastic polyoxymethylene (POM) tube containing degassed water. The wall thickness of the POM tube is 1 mm. A thin film of 40 µm, stretched at the bottom of the POM tube, ensured its insulation from the degassed water. The thin film material was compatible with any cell culture medium. To meet the objective of avoiding wave reflection and considering the constraints in dimensions of cell culture in an incubator (preventing addition of a high amount of water), a 10 mm-thick absorbing foam (Aptflex F28, Precision Acoustics Ltd, Dorchester, UK) was inserted inside the POM tube, 28 mm above the film. The anti-reflection cover was placed over the Petri dish.

In order to adapt the Petri dish/anti-reflection cover set to the *in vitro* ultrasound cell stimulation, the diameters of the Petri dish and of the anti-reflection cover were defined to make gas exchanges with the outside possible. Therefore, the diameters of the Petri dish and of the anti-reflection cover were 60 mm, larger than the diameter of the culture area (of hypothetical cells) of 35 mm.

Finally, the Petri dish/anti-reflection cover set was held above the transducer by means of a holder that was large enough not to interfere with the acoustic field generated by the transducers. The assembly ensures the horizontality of the active face of the transducer, the Petri dish and the anti-reflection cover.

4 Experimental set-up and configurations

The general synoptic diagram of the experiments is presented in Figure 2. The experiment room was air-conditioned and kept at a constant temperature. Experimental conditions did not change during the tests. The experiments in this study were performed successively using two immersion transducers (Imasonic, Voray-sur-l'Ognon, France) of center frequency 1 MHz and 2.25 MHz,

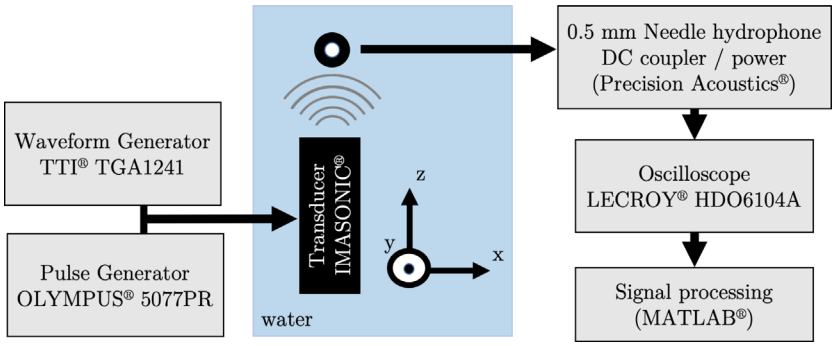

Figure 2. General synoptic diagram.

respectively. The active front diameter and active area were 13 mm and 1.33 cm^2 for the 1 MHz transducer, and were 9.5 mm and 0.71 cm^2 for the 2.25 MHz transducer. The acoustic impedance of the piezo-composite material (Z_{trans}) was 21 MRayls.

Each transducer was powered first by a pulse-receiver generator (Sofranel 5077 PR, Olympus, Waltham, MA 02453, USA) for the calibration of the experiments, and then, by a waveform generator (TGA 1241, Thurlby Thandar Instruments Limited, Huntingdon, UK) to study the performance of the anti-reflection cover under LIUS conditions. The radio-frequency signals (RF-signals) were conveyed from the 12-bit oscilloscope (Lecroy HDO 6104, Teledyne Inc., Thousand Oaks, CA USA) to a personal computer using a USB interface file transfer, and stored. The processing algorithms were implemented using Matlab (The MathWorks, Inc., Natick, MA, USA).

Acoustic pressure measurements were performed in transmission mode using a 0.5 mm needle hydrophone, a submersible wide-band amplifier and a converter-coupler (Precision Acoustics Ltd, Dorchester, UK). According to the technical data sheet provided by the manufacturer, the sensitivity of the needle hydrophone was 426 mV/MPa for the 1 MHz-transducer, and 422 mV/MPa for the 2.25 MHz-transducer.

The transducer and the hydrophone placed above were immersed in a large circular tank (3 m diameter and 1.25 m height) filled with degassed water (ρ_{water} = 1000 kg/m^3). The temperature of the water in the tank (17.8 °C) was determined using a digital thermometer.

The ultrasonic incident wave beam was perpendicular to the water–air interface as well as to the water–dish interface. The ultrasonic wave was therefore transmitted through the Petri dish under normal incident conditions. Only pure compression waves were taken into account, and the shear waves propagating in the walls of the Petri dish were considered negligible. The ultrasonic wave velocities were taken to be constant and independent of the frequency (non-dispersive medium and material).

A micrometric electro-mechanical positioning scanner (precision of 0.1 mm) was used to locate the hydrophone in the 3D-space (x, y, z) from the front face to the far field of the transducer. The distance between the transducer and the water–air interface was defined by D. Its value was estimated by measuring the arrival time of the echo returned by the water–air interface. In all configurations, the hydrophone remained fully immersed. Figure 3 show the different experimental configurations selected for the acoustic measurements:

- *High water level and vertical position of the hydrophone, without (Fig. 3a) and with the Petri dish (no cover) (Fig. 3b)*: This configuration means that there was a high column of water above the transducer (D = 700 mm). The wave reflected from the water–air interface arrived with a significant delay compared with the main incident wave, and was outside the signal recording range.
- *Low water level and horizontal position of the hydrophone, with the Petri dish, without (Fig. 3c) and with (Fig. 3d) the anti-reflection cover*: This configuration modeled a liquid level similar to the one used by biologists in cell culture dishes. The distance D was 46.3 mm.

5 Calibration of the acoustic set-up

For the calibration of the set-up, including the characterization of the acoustic fields of the transducers, and the hydrophone and the Petri dish locations, the chosen configuration was the one presented in Figure 4a. There was no cover over the Petri dish, and the hydrophone was in vertical position. The ultrasonic wave transmission mode was the short-pulse mode described as follows.

5.1 The short-pulse mode

The transmitted input signal was an electric short-pulse signal delivered by the pulse-receiver generator. The pulse repetition frequency $\left(f_{PRF} = \frac{1}{t_{PRP}}\right)$ was 100 Hz, and the gain was fixed at 10 dB. The frequency calibrations of the pulse-receiver generator were 1 MHz and 2.25 MHz, respectively. The mean ultrasonic wave velocity in the tank (c_{water} = 1474 ± 1 m/s) was calculated using the arrival time variation measurements for two distances between each transducer and the water–air interface (Fig. 4a). The attenuation of the ultrasonic waves in water (α_{water}) was 0.0022 dB/cm, whatever the frequency.

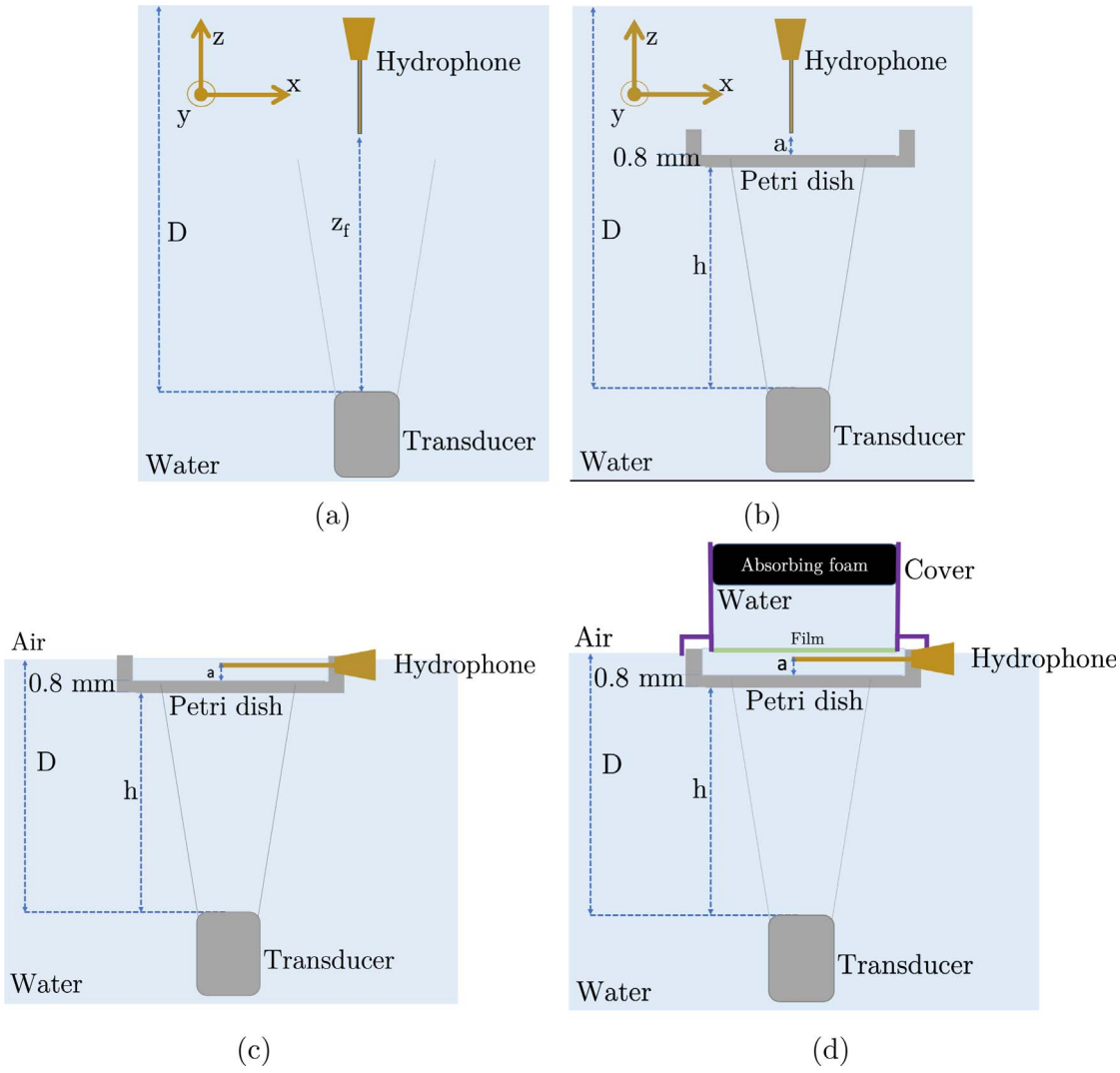

Figure 3. Schematic drawings of *high water level configuration* (a) without and (b) with the Petri dish and *low water level configuration* (c) without and (d) with the anti-reflection cover.

5.2 The acoustic fields and the focal zones

With the micrometric electro-mechanical positioning scanner, the peak acoustic pressure distribution was measured by scanning the *xz*-plane ($y = 0$), with x ranging from -7 to 7 mm, and z ranging from 4 to 45 mm from the front face of the transducer. Figures 4b and 4c (Figs. 4d and 4e) show the axial distribution of the ultrasonic pressure delivered by the 1 MHz-transducer (2.25 MHz-transducer) along the beam axis (z). The depths marking the beginning of the focal zone (in the sense of the definitions of Bushberg et al. [19]) were 20 ± 2 mm for the 1 MHz-transducer and 25 ± 2 mm for the 2.25 MHz-transducer. The lateral apertures were 12 mm and 7 mm, respectively. The theoretical focal length for the 1 MHz-transducer (respectively, for the 2.25 MHz-transducer) was of 29 mm (respectively, 31 mm) at -6 dB, and the corresponding lateral resolution was 13 mm (respectively, 9 mm). The theoretical and experimental values are therefore in agreement.

5.3 Location of the Petri dish

The distance between the transducer and the Petri dish back wall was defined by h. The distance h was chosen so that the Petri dish back wall was located on the maximum acoustic peak pressure of the acoustical fields, that is, 25 mm when using the 1 MHz-transducer, and 36 mm when using the 2.25 MHz-transducer. Its value was estimated using the pulse-echo mode by measuring the arrival time of the echo returned by the Petri dish back wall.

5.4 Locations of the hydrophone

The distance z_f was defined as the distance between the transducer and the tip of the hydrophone, without or with the Petri dish and the anti-reflection cover (Fig. 3).

The distance z_f was 28 mm with the 1 MHz-transducer, and was 39 mm with the 2.25 MHz-transducer, and was constant for all measurement configurations. As shown in

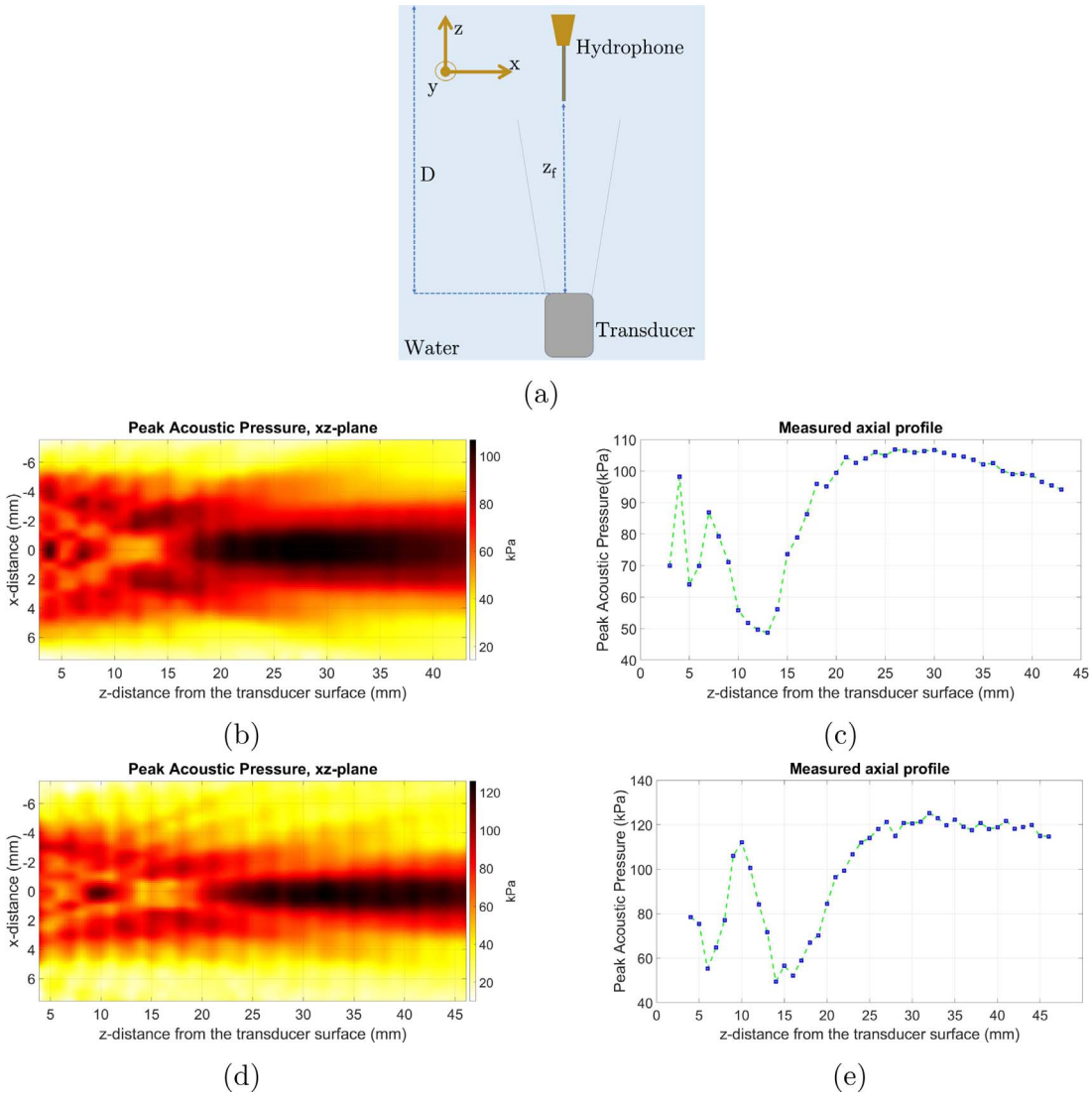

Figure 4. Calibration configuration (a). Pressure distribution in *xz*-plane for the 1 MHz-transducer for free field (b) and along the beam axis (c). Pressure distribution in *xz*-plane for the 2.25 MHz-transducer for free field (d) and along the beam axis (e).

Figures 3c and 3d, the hydrophone was moved from a vertical position (0°) to a horizontal position (90°). This last position allowed measurements in the Petri dish water layer, with and without the anti-reflection cover.

A 4 mm-deep notch was made in the lateral wall of the Petri dish. In vertical and horizontal positions, the tip of the hydrophone was located in the center of the Petri dish at the height $a = 2.2$ mm above the bottom. According to the technical data sheet provided by the manufacturer [20], the frequency-dependent directional response of the hydrophone is angularly wide enough to justify the comparison of the measurements when it is in the vertical position or the horizontal position. The relative amplitude between the two positions was −5 dB for the 1 MHz-transducer, and −10 dB for the 2.25 MHz-transducer. The RF-signals recorded for each position were therefore normalized with respect to these relative amplitudes. Table 1 summarizes all distances and heights for the experiments performed at 1 MHz and 2.25 MHz.

6 Validation of the anti-reflection cover under LIUS conditions

To test the effectiveness of the anti-reflection cover to meet the LIUS requirements, in particular to ensure that the delivered acoustic intensity level corresponds to a Spatial-Average Temporal-Average Intensity, I_{SATA} (9.2) of 30 mW/cm^2, the ultrasonic wave transmission mode was the tone-burst mode described below.

6.1 The tone-burst mode

The temporal source waveforms delivered by the waveform generator were a 1 MHz-burst and a 2.25 MHz-burst signal, with a time duration of 200 µsec. The amplitude of the waveform generator was 9.5 V (peak-to-peak) for the 1 MHz-transducer and 10 V (peak-to-peak) for the 2.25 MHz-transducer (50 Ω). The pulse repetition period (t_{PRP}) was fixed at 1 ms, through a duty cycle (DC) of

Table 1. Table of distances and heights.

Variable	Distance between	Value (mm)
z_f	The transducer[1] and the hydrophone	28 (1 MHz), 39 (2.25 MHz)
D (high water level)	The transducer[1] and the water–air interface	700
D (low water level)	The transducer[1] and the water–air interface	46.3
h	The transducer[1] and the Petri dish[2]	25 (1 MHz), 36 (2.25 MHz)
a	The Petri dish[3] and the hydrophone	2.2

[1] The active front face of the transducer.
[2] The back wall.
[3] The bottom of the Petri dish.

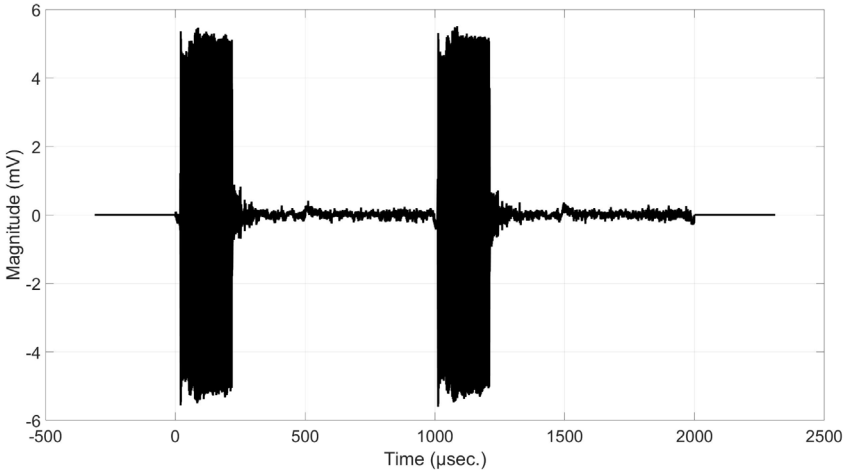

Figure 5. Example of RF-signal recorded by the hydrophone at $z_f = 28$ mm. Configuration: 1 *MHz-transducer*, *high water level*, *vertical position of the hydrophone*.

20%. Figure 5 shows an example of 1 MHz-transmitted RF-signal over two periods, and recorded by the hydrophone at $z_f = 28$ mm, without Petri dish.

6.2 Characterization of the ultrasound intensity distributions under LIUS conditions

The temporal-peak intensity I_{TP}, temporal-average intensity I_{TA}, spatial-peak temporal-average intensity I_{SPTA} and spatial-average temporal-average intensity I_{SATA} [mW/cm^2] (9.2) were measured – the hydrophone being in the vertical position – on a total sounded area around 2.25 cm^2 ($[x, y] = [15$ mm, 15 mm$]$) with a linear pitch of 0.25 mm, at $z_f = 28$ mm for the 1 MHz-transducer and $z_f = 39$ mm for the 2.25 MHz-transducer. Two sets of experiments were conducted for each transducer, without (Fig. 3a) and with (Fig. 3b) the Petri dish, with a high water level ($D = 700$ mm).

The intensity I_{TA} (see Eq. (A.4)) was calculated from the measurement of the peak acoustic pressure p_0 and the intensity I_{TP} (see Eq. (A.3)) following the algorithm proposed by Harris [21] and Preston [22]. I_{SPTA} was the maximum value of the intensity spatial distribution I_{TA} (see Eq. (A.5)), and I_{SATA} was the spatial average of I_{TA} (see Eq. (A.6)) calculated on the −6dB beam area.

Figure 6 shows the I_{TA} distributions for the 1 MHz-transducer. Figure 7 shows the results for the 2.25 MHz-transducer. The circle in the image represents the active front face of the transducer (13 mm). The corresponding I_{SPTA} and I_{SATA} are summarized in Table 2.

This analysis makes it possible to verify that the experimental conditions of insonification in the *high water level* configuration correspond to the values commonly used in LIUS therapy. The I_{SATA} is equal to about 30 mW/cm^2 (31.6 mW/cm^2 at 1 MHz, and 21.9 mW/cm^2 at 2.25 MHz). Note that the I_{SATA} value for the commercial device is generally given with a tolerance of about 30%. The results obtained for the field distributions and for the measurements of I_{SATA} are within this tolerance, and are consequently in accordance with the LIUS conditions.

6.3 The anti-reflection cover similar to a large water column

Figure 8 shows the comparison of transmitted signals between the transducer and the hydrophone in horizontal position for a low water level ($D = 46.3$ mm) without (Fig. 3c) and with (Fig. 3d) the anti-reflection cover, and in vertical position for a high water level ($D = 700$ mm) without the anti-reflection cover (Fig. 3b). Figure 9 shows

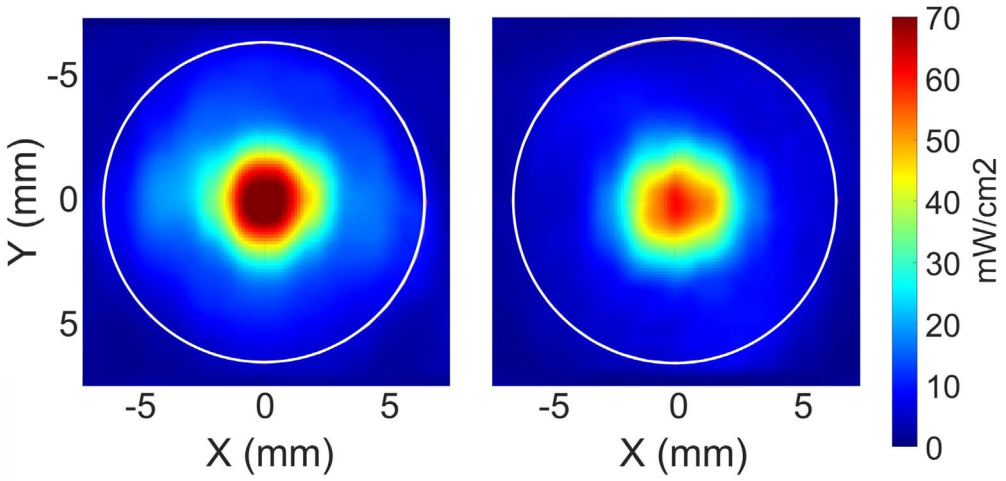

Figure 6. Temporal-average intensity I_{TA} [mW/cm^2] distribution without (left – Fig. 3a) and with (right – Fig. 3b) the Petri dish for 1 MHz-transducer at $z_f = 28$ mm. The white circle represents the area of the transducer.

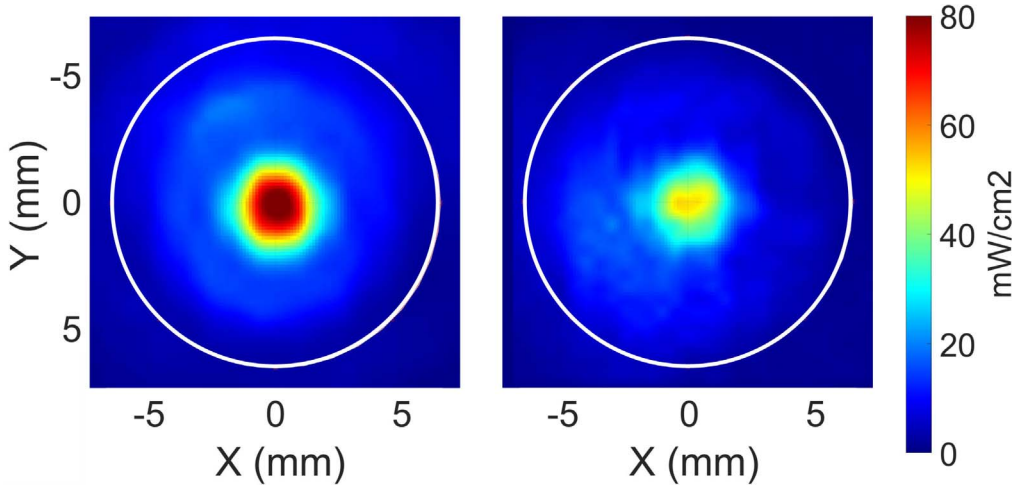

Figure 7. Ultrasound temporal-average intensity distribution I_{TA} [mW/cm^2] without (left – Fig. 3a) and with (right – Fig. 3b) the Petri dish for 2.25 MHz-transducer at $z_f = 39$ mm. The white circle represents the area of the transducer.

Table 2. Measured peak acoustic pressure and intensities.

Frequency/ Configuration	p_0 [kPa]	I_{SPTA} [mW/cm^2]	I^*_{SATA} [mW/cm^2]
1 MHz			
Without Petri dish	103	74.4	37.7
With Petri dish	100.5	60.7	31.6
2.25 MHz			
Without Petri dish	118.5	80.7	42.4
With Petri dish	93.5	51.4	21.9

*−6 dB.

the same results for the 2.25 MHz-transducer. Table 3 summarizes the mean peak acoustic pressures measured for all configurations.

In the *low water level* configuration, the mean peak acoustic pressure was higher without the anti-reflection cover (149 ± 7 kPa at 1 MHz, and 183 ± 5 kPa at 2.25 MHz) than with the anti-reflection cover (105 ± 1 kPa at 1 MHz, and 83.5 ± 0.6 kPa at 2.25 MHz, cf. Tab. 3). Without the anti-reflection cover, the ultrasonic waves were strongly reflected at the water–air interface, which resulted in a dramatic increase in the acoustic pressure in the Petri dish water layer. With the anti-reflection cover, the ultrasonic waves were transmitted inside and partially absorbed by the absorbing foam that prevents multiple reflections by suppressing the water–air interface. The reduction in the mean peak acoustic pressure was 30% at 1 MHz and 54% at 2.25 MHz. The acoustic pressure measured using the hydrophone in the horizontal position, under the anti-reflection cover in the *low water level* configuration, was of the same order of magnitude as that measured when the hydrophone was in a vertical position, without the anti-reflection cover and in the *high water level* configuration (105 ± 3 kPa at 1 MHz, and 86.7 ± 2 kPa at 2.25 MHz, cf. Tab. 3). In summary, there were no more standing waves in the Petri dish water layer

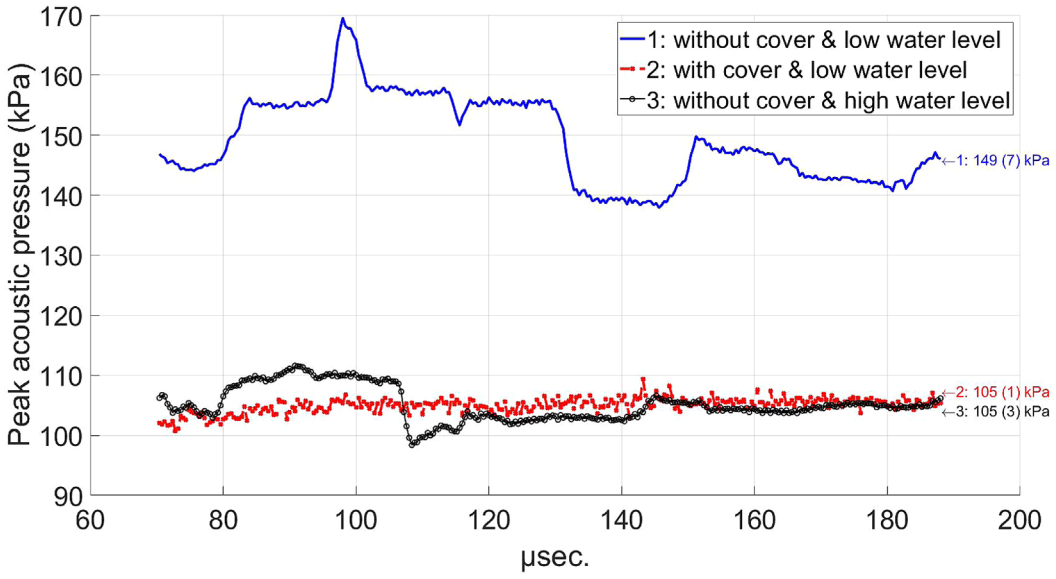

Figure 8. Moduli of the Hilbert transform of the transmitted RF-signals between the 1 MHz-transducer and the hydrophone in horizontal position and a low water level above the Petri dish, and the hydrophone in vertical position and a high water level. On the right, the mean values and standard deviations are mentioned.

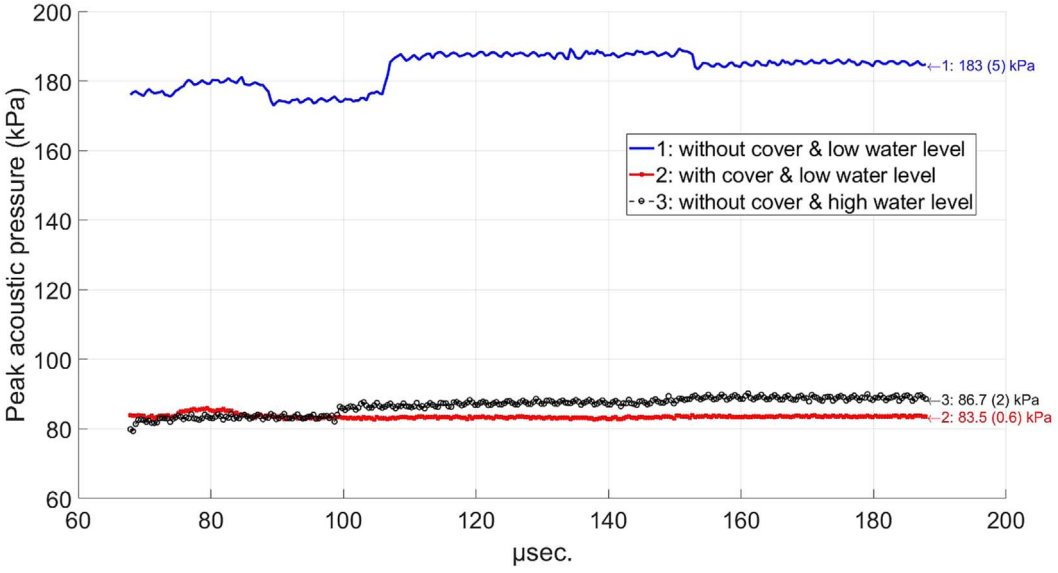

Figure 9. Moduli of the Hilbert transform of the transmitted RF-signals between the 2.25 MHz-transducer and the hydrophone in horizontal position and a low water level above the Petri dish, and the hydrophone in vertical position and a high water level. On the right, the mean values and standard deviations are mentioned.

Table 3. Mean peak acoustic pressure measured, p_0 [kPa].

Frequency MHz	Low water level without cover	Low water level with cover	High water level without cover
1	149 ± 7	105 ± 1	105 ± 3
2.25	183 ± 5	83.5 ± 0.6	86.7 ± 2

when the anti-reflection cover was present, and the intensity delivered was correctly estimated by measuring the mean peak acoustic pressure in the Petri dish water layer with a high water column above. It is worth noting that the presence of the hydrophone in the horizontal position necessarily disturbs the acoustic field. However, as it is present in all configurations, this disturbance is identical, even though, for the configuration with the anti-reflection cover and the 40 μm-film, it could disturb more. The presence of the hydrophone could also explain the high amplitude of

the signals, standing waves being created under the hydrophone. To conclude, the effect of the anti-reflection cover is similar to that of a high water column above the Petri dish, reducing drastically the perturbation induced by the wave reflection at the water–air interface.

6.4 Analytical estimation of the acoustic intensity under the anti-reflection cover

Once the effectiveness of the anti-reflection cover was validated, a quantitative study of the energy transmitted into the water layer was undertaken, and the intensity loss calculated (see Eq. (A.8)). To do so, a comparison between the analytically calculated $[I_{SPTA}]^A$ and measured $[I_{SPTA}]^M$ intensities was conducted. The time duration of the transmitted signal was 200 µsec. Therefore, the propagation distance was about 29.5 cm, which was of the same order of magnitude as the distance between the transducer and the Petri dish back wall (h = 25 mm, and h = 36 mm, Tab. 1). $[I_{SPTA}]^M$ measured at a = 2.2 mm from the bottom of the Petri dish was the result of a sum of several waves that traveled back and forth several times between the transducer and the Petri dish back wall, and inside the bottom thickness of the Petri dish. Therefore, for the analytical calculation, these back-and-forth travels (one *Run* is a one-way path traveled by the ultrasonic wave) were considered. Three runs were reasonable, given the distances between the interfaces. Multiple reflections beyond three runs were not significant. Recordings in reflection and pulse-echo mode (back wall echoes on the Petri dish) were made to analyze the amplitudes of the RF-signals due to the multiple reflections, and beyond four back-and-forth travels (3 + 1 *Runs*) the signals were weak, and slightly out of the noise.

The reflection and transmission coefficients (see Eqs. (A.1) and (A.2)) were calculated at the water–Petri dish interface, at the water–transducer interface, and inside the bottom thickness. The attenuations (see Eq. (A.7)) were taken into account in the water and in the thickness of the Petri dish. The parameters of the study are summarized in Table 4.

The loss of intensity of a wave (see Eq. (A.8)) inside the Petri dish, at a distance z_f along the beam axis of the transducer is presented in Table 5 for the 1 MHz-transducer, and in Table 6 for the 2.25 MHz-transducer. The intensity increases under the Petri dish because of the multiple reflections between the dish and the transducer.

Analytical and measured intensities are similar for both transducers. The differences between the two values are 2.5% (1 MHz) and 6% (2.25 MHz). This result is acceptable and a simple analytical calculation makes it possible to estimate the ultrasound intensity the cells in the culture medium receive.

Table 4. Physical parameters used for the analytical calculation of the intensity loss in the Petri dish water layer as hypothetical cell culture medium.

Physical parameters	Values
c_{water}	1474 ± 1 m/s
ρ_{water}	1000 kg/m^3
Z_{water}	1.47 MRayls
α_{water}	0.0022 dB/cm
c_{dish}	2367 m/s
ρ_{dish}	1040 kg/m^3
Z_{dish}	2.46 MRayls
α_{dish}	1.10 dB/cm (1 MHz)
	1.25 dB/cm (2.25 MHz)
E*	0.8 mm
a**	2.2 mm
$R_{water,dish}$	0.063
Z_{trans}	21 MRayls
$R_{water,transducer}$	0.755

* The bottom thickness of the Petri dish.
** The distance between the bottom of the Petri dish and the hydrophone tip position.

7 Discussion & conclusion

Low intensity ultrasound stimulation is a modality used today in medical therapy for bone regeneration. The performance of the commercial devices used in the clinical field is still being debated. To understand the physical phenomena, laboratory tests are performed on cells placed in Petri dishes and insonified by acoustic waves. Unfortunately, as mentioned in [13], several parameters are liable to compromise the monitoring of the acoustic dose delivered to the cells. Among them, the distance between the transducer and the Petri dish, the coupling medium (degassed water), and the formation of standing waves inside the culture medium. All of them have been treated in the anti-reflection cover device. A fourth one is the relative size of the beam and the dish and the homogeneity of the field delivered inside the Petri dish. This question is in progress. In this work, a custom-designed anti-reflection cover placed on the Petri dish has been developed, whose constituent materials and dimensions are entirely compatible with *in vitro* cell tests in incubators. This anti-reflection cover makes it possible to trap transmitted waves and to avoid the standing waves in the cell culture medium. Therefore, the cell culture medium is comparable to a column of water several centimeters high in which the waves would not be reflected on any interface. Even if the results presented in this paper (Figs. 8 and 9) show the efficiency of the cover, more tests are needed to improve the reproducibility of these results and to obtain a fine interpretation of the interaction of the ultrasonic field with the anti-reflection cover. On this last point, the development of a numerical model reproducing the experimental conditions is in progress and should bring some answers. Thus, the acoustic intensity in the cell culture medium inside the Petri dish/anti-reflection cover set can be estimated by the measurement of an equivalent intensity in a large volume of water above a Petri dish. It is then possible to estimate the energy received by cells under low intensity ultrasound stimulation. This set-up has been designed (dimensions and materials) to allow *in vitro* ultrasound stimulation without having to remove the cell cultures from the incubator. It offers the possibility

Table 5. Analytical calculation of the intensity and loss for the 1 MHz-transducer.

Intensity of the wave		(mW/cm^2)	Intensity loss (%)
Measured at 25 mm (under the Petri dish)		71.6	
Measured at 28 mm (above the Petri dish)	$[I_{SPTA}]^M$	60.7	15.2
Calculated after 3 *Runs* in water		78.4	
Transmitted into the Petri dish		73.5	
Calculated after 3 *Runs* in the bottom thickness	$[I_{SPTA}]^A$	62.3	13

Table 6. Analytical calculation of the intensity and loss for the 2.25 MHz-transducer.

Intensity of the wave		(mW/cm^2)	Intensity loss (%)
Measured at 36 mm (under the Petri dish)		64.5	
Measured at 39 mm (above the Petri dish)	$[I_{SPTA}]^M$	51.4	20.3
Calculated after 3 *Runs* in water		70.6	
Transmitted into the Petri dish		66.1	
Calculated after 3 *Runs* in the bottom thickness	$[I_{SPTA}]^A$	54.7	15.2

to avoid any human manipulation of the cell cultures even in the case of an ultrasound stimulation practiced over several days which is excluded in the configurations proposed in [16] and [10]. This possibility greatly limits the risks of contamination of cell cultures. Moreover the anti-reflection cover is easily adaptable to any current well on water surface whatever its dimensions and even for multiwell plates. Its low cost makes it possible to consider duplicating it for serial studies and achieve the amount of data necessary for statistical analysis of biological results.

Conflict of interest

The authors declare that they have no conflicts of interest in relation to this article.

Acknowledgments

This research was funded by the CNRS project AAP2017-OSEZBARON, and the *A*MIDEX* Fundation of Aix Marseille University. It was carried out within the framework of the Institute for Mechanical Science and Engineering, Aix Marseille University. The doctoral theses of Meysam Majnooni and Elise Doveri are funded by the French Ministry of Research. The authors are grateful to Laurent Sabatier and Olivier Pot from the Laboratory of Mechanics and Acoustics (LMA), Marseille, France.

References

1. T.G. Leighton: What is ultrasound? Progress in Biophysics and Molecular Biology 93, 1 (Jan. 2007) 3–83. ISSN: 00796107. https://doi.org/10.1016/j.pbiomolbio.2006.07.026. [Online]. Available: https://linkinghub.elsevier.com/retrieve/pii/S0079610706000812 (visited on 09/27/2021).
2. W.D. O'Brien: Ultrasound-biophysics mechanisms. Progress in Biophysics and Molecular Biology 93, 1 (Jan. 2007) 212–255. ISSN: 00796107. https://doi.org/10.1016/j.pbiomolbio.2006.07.010. [Online]. Available: https://linkinghub/elsevier.com/retrieve/pii/S0079610706000915 (visited on 09/27/2021).
3. G. Ter Haar: Therapeutic applications of ultrasound. Progress in Biophysics and Molecular Biology 93, 1 (Jan. 2007) 111–129. ISSN: 00796107. https://doi.org/10.1016/j.pbiomolbio.2006.07.005. [Online]. Available: https://linkinghub.elsevier.com/retrieve/pii/S0079610706000836 (visited on 09/27/2021).
4. Z. Izadifar, P. Babyn, D. Chapman: Mechanical and biological effects of ultrasound: A review of present knowledge. Ultrasound in Medicine & Biology 43, 6 (Jun. 2017) 10851104.ISSN: 03015629. https://doi.org/10.1016/j.ultrasmedbio.2017.01.023. [Online]. Available: https://linkinghub.elsevier.com/retrieve/pii/S0301562917300522 (visited on 09/24/2021).
5. P. Aspenberg: Is LIPUS the baby in the bathwater?: Comment to a BMJ editorial. Acta Orthopaedica 88, 1 (Jan. 2017) 1–1. ISSN: 1745-3674, 1745-3682. https://doi.org/10.1080/17453674.2016.1269273. [Online]. Available: https://www.tandfonline.com/doi/full/10.1080/17453674.2016.1269273 (visited on 10/08/2019).
6. R.W. Poolman, T. Agoritsas, R.A.C. Siemieniuk, I.A. Harris, I.B. Schipper, B. Mollon, M. Smith, A. Albin, S. Nador, W. Sasges, S. Schandelmaier, L. Lytvyn, T. Kuijpers, L.W.A.H. van Beers, M.H.J. Verhofstad, P.O. Vandvik: Low intensity pulsed ultrasound (LIPUS) for bone healing: A clinical practice guideline, BMJ 356 (Feb. 2017) jJ576. ISSN: 0959-8138, 1756-1833. https://doi.org/10.1136/bmj.j576. [Online]. Available: https://www.bmj.com/lookup/doi/10.1136/bmj.j576 (visited on 09/27/2021)..
7. S. Schandelmaier, A. Kaushal, L. Lytvyn, D. Heels-Ansdell, R.A.C. Siemieniuk, T. Agoritsas, G.H. Guyatt, P.O. Vandvik, R. Couban, B. Mollon, J.W. Busse: Low intensity pulsed ultrasound for bone healing: Systematic review of randomized controlled trials. BMJ (Clinical research ed.) 356 (Feb. 2017) j656. ISSN: 1756-1833. https://doi.org/10.1136/bmj.j656.
8. F. Padilla, R. Puts, L. Vico, K. Raum: Stimulation of bone repair with ultrasound: A review of the possible mechanic effects. Ultrasonics 54, 5 (Jul. 2014) 1125–1145. ISSN: 0041624X. https://doi.org/10.1016/j.ultras.2014.01.004. [Online]. Available: http://linkinghub.elsevier.com/retrieve/pii/S0041624X14000055 (visited on 10/03/2016).
9. R. Puts, K. Ruschke, T.H. Ambrosi, A. Kadow-Romacker, P. Knaus, K.V. Jenderka, K. Raum: A focused low-intensity pulsed ultrasound (FLI- PUS) system for cell stimulation: Physical and biological proof of principle. IEEE Transactions on Ultrasonics, Ferroelectrics, and Frequency Control

63, 1 (Jan. 2016) 91–100. ISSN: 0885-3010. https://doi.org/10.1109/TUFFC. 2015.2498042. [Online]. Available: http://ieeexplore.ieee.org/document/7317777/ (visited on 07/25/2017).
10. F. Fontana, F. Iberite, A. Cafarelli, A. Aliperta, G. Baldi, E. Gabusi, P. Dolzani, S. Cristino, G. Lisignoli, T. Pratellesi, E. Dumont, L. Ricotti: Development and validation of low-intensity pulsed ultrasound systems for highly controlled in vitro cell stimulation. Ultrasonics 116 (Sep. 2021) 106495. ISSN: 0041624X. https://doi.org/10.1016/j.ultras.2021.106495. [Online]. Available: https://linkinghub.elsevier.com/retrieve/pii/S0041624X21001268 (visited on 09/27/2021).
11. K. Hensel, M.P. Mienkina, G. Schmitz: Analysis of ultrasound fields in cell culture wells for in vitro ultrasound therapy experiments. Ultrasound in Medicine & Biology 37, 12 (2011) 2105–2115.
12. W. Secomski, K. Bilmin, T. Kujawska, A. Nowicki, P. Grieb, P. A. Lewin: In vitro ultrasound experiments: Standing wave and multiple reflections influence on the outcome. *Ultrasonics* 77 (May 2017) 203–213. ISSN: 0041624X. https://doi.org/10.1016/j.ultras.2017.02.008. [Online]. Available: https://linkinghub.elsevier.com/retrieve/pii/S0041624X16303109 (visited on 10/27/2021).
13. M. Snehota, J. Vachutka, G. ter Haar, L. Dolezal, H. Kolarova: Therapeutic ultrasound experiments in vitro: Review of factors influencing outcomes and reproducibility. Ultrasonics 107 (Sep. 2020) 106167. ISSN: 0041624X. https://doi.org/10.1016/j.ultras.2020.106167. [Online]. Available: https://linkinghub.elsevier.com/retrieve/pii/S0041624X20301062 (visited on 10/27/2021).
14. J.J. Leskinen, H.M. Karjalainen, A. Olkku, K. Hynynen, A. Mahonen, M.J. Lammi: Genome-wide microarray analysis of mg-63 osteoblastic cells exposed to ultrasound. Biorheology 45, 3–4 (2008) 345–354.
15. C.-H. Lai, S.-C. Chen, L.-H. Chiu, C.-B. Yang, Y.-H. Tsai, C.S. Zuo, W.H.-S. Chang, W.-F. Lai: Effects of low-intensity pulsed ultrasound, dexamethasone/tgf-ß1 and/or bmp-2 on the transcriptional expression of genes in human mesenchymal stem cells: Chondrogenic vs. osteogenic differentiation. Ultrasound in Medicine & Biology 36, 6 (2010) 1022–1033.
16. L. Zhao, Y. Feng, H. Hu, A. Shi, L. Zhang, M. Wan: Low-intensity pulsed ultrasound enhances nerve growth factor-induced neurite outgrowth through mechanotransduction-mediated ERK1/2-CREB-Trx-1 signaling. Ultrasound in Medicine & Biology 42, 12 (Dec. 2016) 2914–2925. https://doi.org/10.1016/j.ultrasmedbio.2016.07.017.
17. A.R. Salgarella, A. Cafarelli, L. Ricotti, L. Capineri, P. Dario, A. Menciassi: Optimal ultrasound exposure conditions for maximizing c2c12 muscle cell proliferation and differentiation. Ultrasound in Medicine & Biology 43, 7 (2017) 1452–1465.
18. K. Metwally, E. Lefevre, C. Baron, R. Zheng, M. Pithioux, P. Lasaygues: Measuring mass density and ultrasonic wave velocity: A wavelet-based method applied in ultrasonic reflection mode. *Ultrasonics* 65 (Feb. 2016) 10–17. ISSN: 0041624X. https://doi.org/10.1016/j.ultras.2015.09.006. [Online]. Available: http://linkinghub.elsevier.com/retrieve/pii/S0041624X15002292 (visited on 09/06/2018).
19. J.T. Bushberg (Ed.): The essential physics of medical imaging, 3rd edn. Wolters Kluwer Health/Lippincott Williams & Wilkins, Philadelphia, 2012, p. 1030. ISBN: 978-0-7817-8057-5.
20. G. Livingstone: Precision acoustics technical data sheet (nh0500). 2016. [Online]. Available: https://bit.ly/35H74cc.
21. G.R. Harris: A discussion of procedures for ultrasonic intensity and power calculations from miniature hydrophone measurements. Ultrasound in Medicine & Biology 11, 6 (Nov. 1985) 803–817. ISSN: 03015629. https://doi.org/10.1016/0301-5629(85)90074-2. [Online]. Available: https://linkinghub.elsevier.com/retrieve/pii/0301562985900742 (visited on 11/06/2020).
22. R.C. Preston: Output measurements for medical ultrasound. Springer, London, London, 1991. OCLC: 958523120, ISBN: 978-1-4471-1883-1. [Online]. Available: http://public.eblib.com/choice/publicfullrecord.aspx?p=3075057 (visited on 08/30/2017).
23. N.C. on Radiation Protection Measurements (Ed.): *Biological effects of ultrasound: mechanisms and clinical implications,* NCRP report no. 74. The Council, Bethesda, MD, 1983, p. 266. ISBN: 978-0-913392-64-5.

Appendix

A Wave coefficients and intensities

A.1 Reflection and transmission coefficients

The reflection coefficient of a wave on a medium 1/medium 2 interface is defined under normal incident conditions as:

$$R_{1,2} = \frac{[Z_2 - Z_1]^2}{[Z_2 + Z_1]^2}, \tag{A.1}$$

and the transmission coefficient is defined as:

$$T_{1,2} = \frac{4Z_1Z_2}{[Z_2 + Z_1]^2}, \tag{A.2}$$

where $Z_1 = \rho_1 c_1$ and $Z_2 = \rho_2 c_2$ are the acoustic impedances [MRayls] of medium 1 and of medium 2. ρ is the mass density [kg/m^3] of the medium, and c is the ultrasonic wave velocity [m/s] propagating in the medium.

A.2 Acoustic intensities

The methods for assessing acoustic intensities were proposed by Harris [21] and Preston [22]. There are several definitions of useful acoustic intensities referenced by international authorities [23], including the temporal-peak intensity I_{TP} [mW/cm^2] which describes the distribution of the acoustic pressure of a wave over time, at the position z along the beam axis, and which is calculated as:

$$I_{\mathrm{TP}}(z) = \frac{< p_0^2(z) >}{Z} = \frac{< \max[p^+(z), p^-(z)]^2 >}{Z}, \tag{A.3}$$

Z is the acoustic impedance of the medium. The peak acoustic pressure p_0 [kPa] is therefore assumed to be the greater of the two values between the maximum peak acoustic pressure p^+ (i.e., maximum voltage of the recorded signal) and the minimum peak acoustic pressure p^- (i.e., minimum voltage of the recorded signal). The Temporal-Average Intensity I_{TA} [mW/cm^2] is the intensity I_{TP} over the total time of the ultrasonic insonification, equal to the ratio between the pulse/burst duration t_{pulse} and the pulse repetition period t_{PRP}:

$$I_{\mathrm{TA}}(z) = I_{\mathrm{TP}}(z)\frac{t_{\mathrm{pulse}}}{t_{\mathrm{PRP}}}. \tag{A.4}$$

By cross-referencing spatial and temporal considerations, several intensities can be defined. The spatial-peak temporal-average intensity I_{SPTA} [mW/cm^2] is the maximum intensity in the spatial field cross-section at a distance z_f from the front face of the transducer:

$$I_{\mathrm{SPTA}}(z_f) = \max_{x,y}\big(I_{\mathrm{TA}}(z_f)\big), \tag{A.5}$$

where x and y are the coordinates of the points on the surface.

The spatial-average temporal-average intensity I_{SATA} [mW/cm^2] is the measure of intensity I_{TA} per unit area at the distance z_f from the front face of the transducer:

$$\begin{aligned} I_{\mathrm{SATA}}(z_f) &= \frac{1}{N}\sum_{x,y=1}^{N}\left[I_{\mathrm{TA}}(z_f)\right]_{x,y},\ \left[I_{\mathrm{TA}}\right]_{x,y} \\ &\geq 0.25 \times \left[I_{\mathrm{SPTA}}\right]_{x,y}. \end{aligned} \tag{A.6}$$

A.3 Intensity loss

The intensity $I(z_2)$ of a wave at the distance z_2 is function of the initial intensity $I(z_1)$ and the attenuation coefficient α of the wave over the distance $|z_2 - z_1|$:

$$I(z_2) = I(z_1)\exp\left(-2\alpha|z_2 - z_1|\right). \tag{A.7}$$

The intensity loss is expressed as a percentage (%) of the intensity lost:

$$I_{\mathrm{loss}} = 100 \times \frac{I(z_1) - I(z_2)}{I(z_1)}. \tag{A.8}$$

Cite this article as: Majnooni M. Doveri E. Baldisser J. Long V. Houles J, et al.. 2022. Anti-reflection cover to control acoustic intensity in *in vitro* low-intensity ultrasound stimulation of cells. Acta Acustica, **6**, 11.